

Ellipsometry of light scattering from multilayer coatings

C. Deumié, H. Giovannini, and C. Amra

A scatterometer is extended and allows us to perform ellipsometric measurements on scattered light in each direction of space. Experimental data are given for single thin-film layers and optical coatings and reveal unexpected results. The phenomena are investigated by means of the electromagnetic theories of surface and bulk scattering that emphasize the role of partial correlation and localized defects.
© 1996 Optical Society of America

Key words: Scattering, ellipsometry, surface roughness, bulk inhomogeneity, thin films, optical coatings, localized defects, cross correlation, polarization ratio.

1. Introduction

Many studies have been devoted to the study of light scattering^{1–5} and allow us to improve our knowledge of microstructural parameters such as interface roughnesses^{6,7} and bulk inhomogeneities^{8–10} within optical multilayers. However, these studies are based mainly on the intensity of the scattered light, whereas phase measurements may provide additional and important information when scattering data are analyzed, in particular for the detection of the origin of scattering. In this paper we modify a well-known scatterometer¹¹ in order to build an angle-resolved ellipsometer that allows us to measure phase variations of scattered light in each direction of space.

As discussed in previous papers,^{6,7} the inverse problem of scattering from optical coatings can be solved in many situations with the help of wavelength variations^{4,12} of scattering, spectral isotropy degree of roughness,^{6,7} coatings produced under oblique deposition,^{6,7} rough and supersmooth substrates,⁴ deposition of opaque layers,⁷ etc. More recently the measurement of the polarization ratio¹⁰ of scattered light was shown to be an adequate tool¹³ for

separating surface and bulk effects, provided that the electromagnetic theories can be developed and accurate measurements can be performed. In fact, ellipsometric measurements are a direct continuation of this latter work,^{10,13} as they involve all polarization states of scattering, resulting in a polarimetric phase difference between the scattered waves. In this paper we show how to use these angular phase variations in the study of inverse problems. In particular, separation^{10,13} of surface and bulk scattering is analyzed further, as well as the role of localized defects.^{4,13} In a more general way, we discuss the improvement that is brought about by the introduction of ellipsometric measurements in the study of light scattering.

In the first step the experimental procedure is checked and validated by means of classical reflection ellipsometry measurements on thin-film multilayers produced by ion-assisted deposition and ion plating. The performances and limits of the apparatus are pointed out.

In the second step the procedure is extended to light scattering and the results are analyzed in detail. The technique is highly sensitive and allows us to underline the effects that are due to the correlation between the irregularities within the stack. The influence of second-order terms that occur in the scattering process are also evaluated.

2. Specular Ellipsometry

Reflection ellipsometry measurements^{14,15} are basically used to extract information on the samples investigated, such as thickness, refractive index, and transition layers. In the field of thin-film multilayers, reflection ellipsometry combined with spectro-

The authors are with the Laboratoire d'Optique des Surfaces et des Couches Minces, Unité de Recherche Associée au Centre National de la Recherche Scientifique 1120, Ecole Nationale Supérieure de Physique de Marseille, 13397 Marseille Cedex 20, France.

Received 22 November 1995; revised manuscript received 18 March 1996.

0003-6935/96/285600-09\$10.00/0

© 1996 Optical Society of America

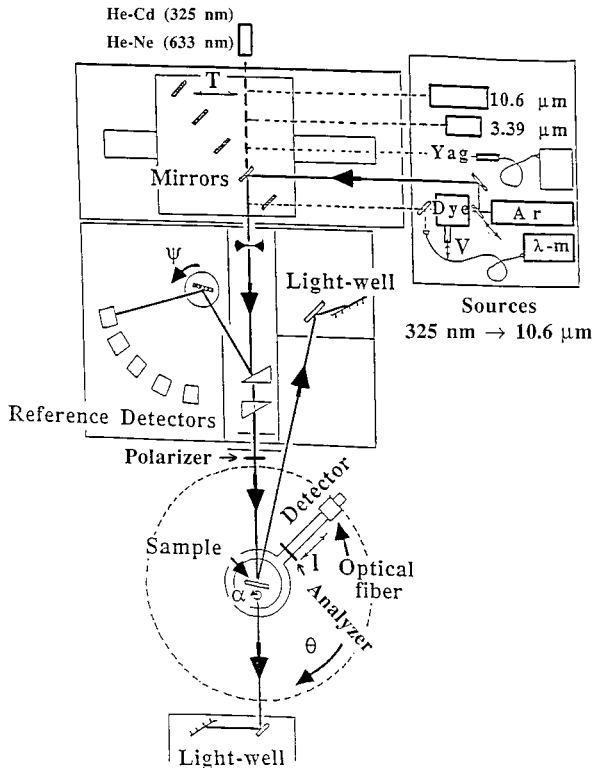


Fig. 1. Schematic view of the scatterometer¹¹ that was extended, by means of the addition of a rotating polarizer and analyzer, to an angle-resolved ellipsometer. Ten axis are fully computer controlled in this experimental setup. Specular and diffuse measurements can be performed at different incidence and scattering angles. Several sources can be used with wavelengths from the UV (325 nm) to the mid-IR (10.6 μm).

scopic measurements can help us to recover the values of both the thickness and the dispersion law of refractive index of each layer.¹⁶ Many configurations^{14,15} can be used to perform these measurements, depending on the residual polarization rate of the source, the polarization sensitivity of the detector, the imperfections of the optical components, and the sensitivity to be obtained.

In the case of our study, the arrangement of the ellipsometer must be compatible with the configuration of the scatterometer previously developed in the laboratory.¹¹ To use the same arrangement of the experimental setup for reflection ellipsometry and for scattering ellipsometry, we have implemented a rotating analyzer ellipsometer (see Fig. 1). Although the theory and procedure are well known for such specular ellipsometry, in the first step we prefer to come back to the basic principles before we introduce and discuss scattering ellipsometry further in the text. For this purpose the analyzer is rotated at low frequency and the parameters are recovered with no use of a Fourier transform.

A. Basic Principles

In the setup of Fig. 1, an incident laser beam strikes a polarizer and an analyzer before and after reflection, respectively, at variable incidence (i) on the

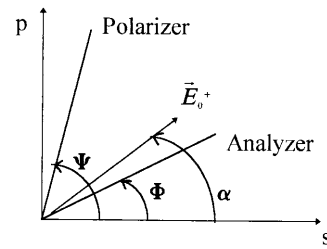


Fig. 2. Rotational azimuth angles of polarizer (ψ) and analyzer (ϕ). The angle (α) gives the direction of the incidence linear polarization.

sample under study. The rotational azimuth angles of polarizer and analyzer are denoted by ψ and ϕ , respectively (Fig. 2), and measured from the direction of the s linear polarization parallel to the surface sample (Fig. 3). The incident beam is assumed to have linear polarization with amplitude E_0^+ and direction α given in Fig. 2.

The sample is a multilayer thin film with materials assumed to be linear, isotropic, homogeneous, and nonmagnetic. All fields are monochromatic and complex in Maxwell equations, with a temporal dependence described by $\exp(-j\omega t)$. Under these conditions the electric field after the polarizer is given by its two s and p components:

$$E_s = E_0^+ \cos \psi \cos(\psi - \alpha), \quad (1a)$$

$$E_p = E_0^+ \sin \psi \cos(\psi - \alpha). \quad (1b)$$

After the analyzer, the amplitude of the two s and p components are added and the resulting electric field is given by

$$E^* = r_s E_s \cos \phi + r_p E_p \sin \phi, \quad (2)$$

that is,

$$E^* = E_0^+ \cos(\psi - \alpha)(r_s \cos \psi \cos \phi + r_p \sin \psi \sin \phi), \quad (3)$$

where $r_s(i)$ and $r_p(i)$ are the amplitude or the complex reflection coefficients of the sample at incidence (i) for each polarization:

$$r_s = \exp(j\delta_s) \sqrt{R_s}, \quad (4a)$$

$$r_p = \exp(j\delta_p) \sqrt{R_p}. \quad (4b)$$

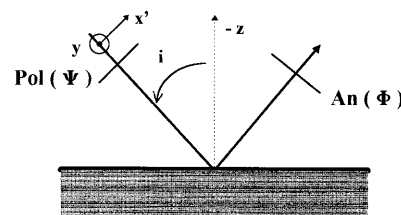


Fig. 3. Illumination procedure at incidence (i) on the sample. y is the direction of the s polarization, and x' is that of p polarization. The normal sample is parallel to z .

Therefore the intensity is given by

$$I = E^* \bar{E}^* = I_0(\psi, \alpha) F(R_s, R_p, \psi, \phi), \quad (5)$$

where

$$I_0 = E_0^{+2} \cos^2(\psi - \alpha), \quad (6)$$

which can be reduced to

$$I_0 = E_0^{+2}/2 \quad (7)$$

when the incident beam is nonpolarized (random alpha angles). Although azimuth angles ψ and ϕ play an equivalent role, the function F is chosen to be

$$F(\psi, \phi) = A(\psi) \cos^2 \phi + B(\psi) \sin^2 \phi + C(\psi) \sin(2\phi), \quad (8)$$

where

$$A(\psi) = R_s \cos^2 \psi, \quad (9a)$$

$$B(\psi) = R_p \sin^2 \psi, \quad (9b)$$

$$C(\psi) = \cos \delta \sqrt{AB}. \quad (10)$$

In Eqs. (9a)–(10) R_s and R_p are the intensity reflection coefficients of the sample, and

$$\delta = \delta_s - \delta_p, \quad (11)$$

the polarimetric phase difference between the two complex reflection factors.

Function F can also be rewritten as

$$2F/A = G(\phi) = \alpha + \beta \cos(2\phi - \gamma), \quad (12)$$

where

$$\alpha = 1 + u, \quad (13a)$$

$$\beta = (1 - u)/\cos \gamma, \quad (13b)$$

$$\tan \gamma = 2 \cos \delta \sqrt{u}/(1 - u), \quad (13c)$$

$$u = B/A. \quad (13d)$$

For a given angular position ψ of the analyzer, function $G(\phi)$ supports extrema

$$G_{\text{extr}} = \alpha \pm \beta \quad (14)$$

at angles

$$\phi_m = (1/2)(\gamma + k\pi). \quad (15)$$

Therefore the polarimetric phase δ could be basically deduced from Eq. (12) and direct measurements made of locations and amplitudes of the extrema of G .

However, the key point in ellipsometry concerns the sensitivity and accuracy of the measurements, for which reason we prefer to fit the measurements with function $F(\phi)$ or $G(\phi)$ and reach parameters (A, B, C) or (α, β, γ) that give the phase term δ from

$$\cos \delta = C/\sqrt{AB} = \beta \sin \gamma/[2(\alpha - 1)^{1/2}]. \quad (16)$$

Therefore the tracking method,¹⁴ which is described below, is used:

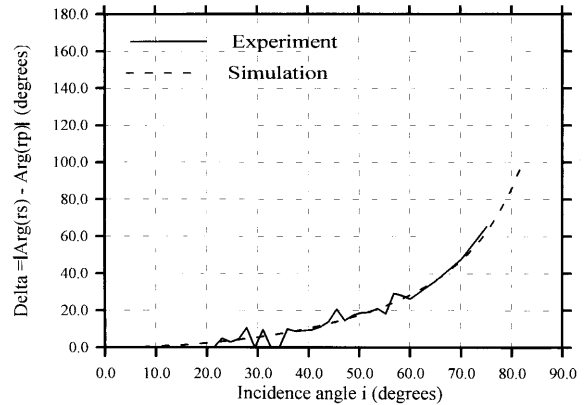


Fig. 4. Comparison between theory and measurement for an opaque Al layer. δ is the reflection ellipsometric phase term plotted versus the incidence angle (i) and given between 0° and 80° . The incident source is a He-Ne laser at 633 nm.

- In the first step curve $F(\phi)$ is recorded with the polarizer angle equal to $\psi = 45^\circ$ and fitted with relation (8). The ratio $A/B = R_s/R_p$ gives the optimal angle ψ_{opt} of the polarizer, with

$$\tan \psi_{\text{opt}} = (R_s/R_p)^{1/2}. \quad (17)$$

- In the second step curve $F(\phi)$ is recorded again with this optimal angle ψ_{opt} . In this case,

$$F/A = 1 + \cos \delta \sin 2\phi, \quad (18)$$

$$A = R_s R_p / (R_s + R_p) \quad (19)$$

and F is fitted with Eq. (18), which gives the phase term δ . No calibration is required.

B. Application to Experiment

To test the procedure and the experimental setup we compare theory and measurements in the case of a single metallic layer and a multodielectric coating.

In Fig. 4 the phase term $\delta(i)$ was measured at the 633-nm wavelength as a function of the incidence angle (i) on an opaque (150-nm-thick) Al layer deposited on a glass substrate by electron-beam evaporation. As shown in this figure, the agreement between theory and experiment is rather successful because the sample was of low quality. The complex index of Al was chosen in the calculation as

$$n = 0.8 + j6 \text{ with } j^2 = -1.$$

A better agreement could be found by fitting the measurements and obtaining a more accurate value for the Al complex refractive index, but such an inverse problem is not our purpose here.

In Fig. 5 the sample under study at 633 nm has a design given as HLHLH(6L)HLHLH, where H and L designate quarter-wave high- and low-index layers at the 645-nm wavelength. The materials are TiO_2 and SiO_2 produced by ion-assisted deposition. With this sample the agreement is also successful, as the

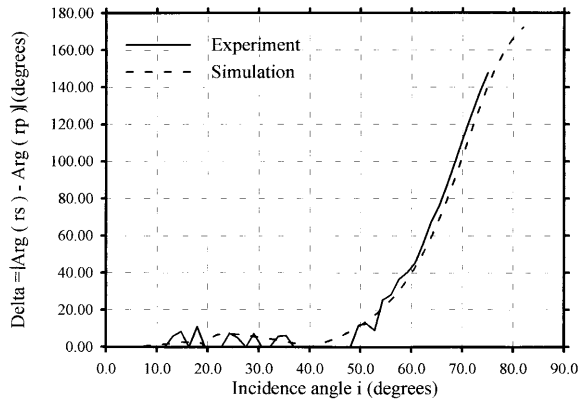


Fig. 5. Same as Fig. 4, but the sample is a multodielectric coating of design HLHLH(6L)HLHLH (see text).

slight differences can be attributed to slight errors in the design.

C. Performances and Limits of the Apparatus

In Section 3 we deal with diffuse ellipsometry and discuss some anomalies that are pointed out by measurements. To introduce the discussion and eliminate artifacts of measurements, we first emphasize the performances and limits of the setup here.

Measurements of $F(\phi)$ in the absence of polarizer and sample gives a constant curve within less than a 1% variation, which indicates a polarization ratio of the incident source of less than 1%. In the absence of sample, cross-polarization measurements give an extinction ratio of better than 10^4 , which corresponds to the efficiency of the setup, including the quality of the laser beam, the polarizer, and the analyzer.

In Fig. 6 we present the measured function $F(\phi)$ recorded at incidence $i = 20^\circ$ for sample HLHLH(6L)HLHLH of Fig. 5. The corresponding fit in Fig. 6 gives a phase term $\delta = 0^\circ$. The electronic noise is less than 10^{-7} in this figure, which gives the detectivity of the system. We note that the dynamic range of experimental data is quasi-identical to the

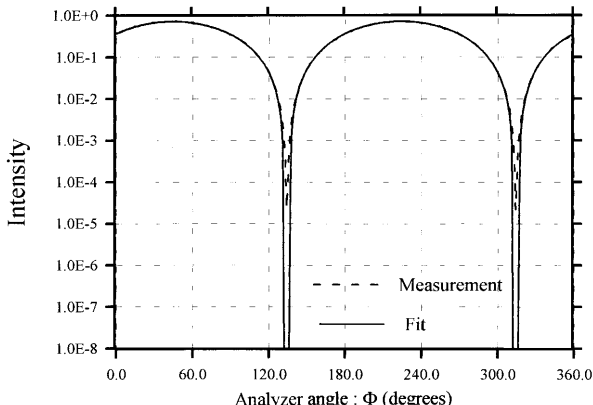


Fig. 6. Function $F(\phi)$ measured at $i = 20^\circ$ incidence for the multodielectric sample of Fig. 5, with the corresponding fit. The phase term δ is 0° . Vertical units are arbitrary.

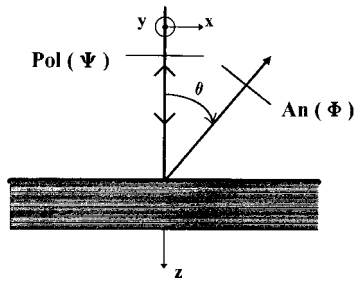


Fig. 7. Schematic view of scattering ellipsometry. The incidence angle (i) is fixed, while ellipsometric measurements are performed on light scattering at each direction θ in space.

10^4 extinction ratio of the crossed polarizer and analyzer.

All these results allow us to validate the experimental setup and directly address the problem of scattering ellipsometry.

3. Diffuse Ellipsometry

In this section we are concerned with diffuse or off-specular ellipsometry (Fig. 7).

A. Surface and Bulk Scattering from Multilayer Optics: Basic Principles

The theory of scattering from multilayer coatings can be found in other previous papers.^{3,8,9} This scattering consists in an off-specular energy resulting from the presence of surface roughness and bulk inhomogeneity within the stacks. For high-quality coatings, the theory may be first-order limited and leads to the following formula¹⁰ for the scattered electric field A that merges in air in direction θ :

$$A = \sum_{i=0}^M C_i^r h_i \quad \text{for surface scattering,} \quad (20)$$

$$A = \sum_{i=1}^M C_i^b p_i \quad \text{for bulk scattering,} \quad (21)$$

where M is the number of layers in the stack, $h_i(\sigma)$ is the Fourier transform of surface profile $h_i(\mathbf{r})$, and $p_i(\sigma)$ is the Fourier transform of the relative transverse variations $\Delta\epsilon_i(\mathbf{r})/\epsilon_i$ in the permittivity of bulk (i). The optical factors C_i^r and C_i^b do not depend on structural irregularities, but they are calculated in connection with the origin of scattering.^{9,10} For surface scattering, C_i^r is obtained by means of a Fourier transform of the discontinuities of the electromagnetic field at the interfaces.^{9,10} For bulk scattering, C_i^b is obtained through the introduction of Green's functions developed in the Fourier plane.^{9,10} Both coefficients depend on the coating design, polarization, wavelength, and incidences.

B. Cross-Correlation Laws

In the field of light scattering from multilayer optics, cross-correlation laws^{4,6,7,12} play a major role and can be described as follows⁶:

- For surface scattering, successive interfaces (i) and ($i + 1$) follow the relation

$$h_i = (1/4\pi^2)a_i * h_{i+1} + g_i, \quad (22)$$

where the first convolution product describes a replication effect of the previous interface and the second term takes into account addition of residual roughness brought by layer ($i + 1$) at interface (i). From this relation the profile at surface (j) can be split into⁶

$$h_j = \alpha'_{jp} h_p + \sum_{k=0}^{p-j-1} \alpha_{j,j+k} g_{j+k}, \quad (23)$$

where the first and the second terms characterize substrate and material effects, respectively.⁶

- The bulk correlation can be described in the same way, even though we have poor knowledge of how the bulk inhomogeneity can be reproduced from one bulk to another or brought to each bulk by materials.^{13,17}

C. Equations for Diffuse Ellipsometry

First-order theory predicts the absence of cross-polarized scattering in the incidence plane. In other words, surface or bulk scattering in the incidence plane at any direction θ is $s(p)$ polarized when the incident beam is $s(p)$ polarized, which can be summarized as

$$A_s = A_{ss} + A_{sp} \quad \text{with } A_{sp} = 0 \text{ in the incidence plane,} \quad (24)$$

$$A_p = A_{pp} + A_{ps} \quad \text{with } A_{ps} = 0 \text{ in the incidence plane.} \quad (25)$$

In these relations, A_u indicates scattering that is due to a (u) polarized incident beam, and A_{uv} designates (v) polarized scattering that is due to a (u) polarized incident beam.

Therefore the equations for diffuse ellipsometry in the incidence plane are strictly analogous to those of specular ellipsometry. We still assume, as in Section 2, that the incident field E_0^+ has a linear polarization given by angle α (Fig. 2). The two polarization states (E_s and E_p) of this field after the polarizer are still given by Eq. (1). When striking the sample, each incident component creates a scattered field (A_s or A_p) in direction θ without any change of polarization, that is,

$$A_s = \nu_s E_s, \quad (26)$$

$$A_p = \nu_p E_p, \quad (27)$$

where ν_s and ν_p are other scattering coefficients that give the scattered field that is proportional to the incident field. It is clear that all relations given above for reflection ellipsometry remain valid for diffuse ellipsometry, provided that the complex reflection coefficients $r_s(i)$ and $r_p(i)$ are replaced by the complex scattering coefficients $\nu_s(\theta)$ and $\nu_p(\theta)$. We

obtain, after the analyzer,

$$A^* = \nu_s E_s \cos \phi + \nu_p E_p \sin \phi, \quad (28)$$

that is,

$$A^* = E_0^+ \cos(\psi - \alpha)(\nu_s \cos \psi \cos \phi + \nu_p \sin \psi \sin \phi), \quad (29)$$

where

$$\nu_s = \sqrt{N_s} \exp(j\eta_s), \quad (30)$$

$$\nu_p = \sqrt{N_p} \exp(j\eta_p). \quad (31)$$

The intensity is given as

$$I = A^* \bar{A}^* = I_0(\psi, \alpha) F(N_s, N_p, \psi, \phi), \quad (32)$$

where

$$I_0 = E_0^{+2}/2 \quad (33)$$

for random incidence polarization, and

$$F(\psi, \phi) = A(\psi) \cos^2 \phi + B(\psi) \sin^2 \phi + C(\psi) \sin(2\phi), \quad (34)$$

where

$$A = N_s \cos^2 \psi, \quad (35)$$

$$B = N_p \sin^2 \psi, \quad (36)$$

$$C = \cos \eta \sqrt{AB}, \quad (37)$$

In this case,

$$\eta = \eta_s - \eta_p \quad (38)$$

is the polarimetric phase difference between the two complex waves scattered in direction θ . Function $F(\phi)$ can also be turned into $G(\phi)$, as in the case of specular ellipsometry [see relations (12)–(19)], and we use the experimental procedure already described in Section 2, with

$$F/A = 1 + \cos \eta \sin 2\phi \quad (39)$$

for the optimal angle of the polarizer.

D. Theoretical Prediction: The Case of Perfect Correlation

First we note from Eqs. (20) and (21) that the surface scattering coefficient ν_s or ν_p of relations (26) and (27) can be written as

$$\nu_{s \text{ or } p} = \sum C_i(s \text{ or } p) h_i, \quad (40)$$

where

$$C_i(s \text{ or } p) = C_i^r(s \text{ or } p)/E_{s \text{ or } p}. \quad (41)$$

In this relation all C and E terms are polarization dependent, except the structural terms h_i .

For a single surface we obtain, for s polarization,

$$\nu_s = C_0(s) h_0 \quad (42)$$

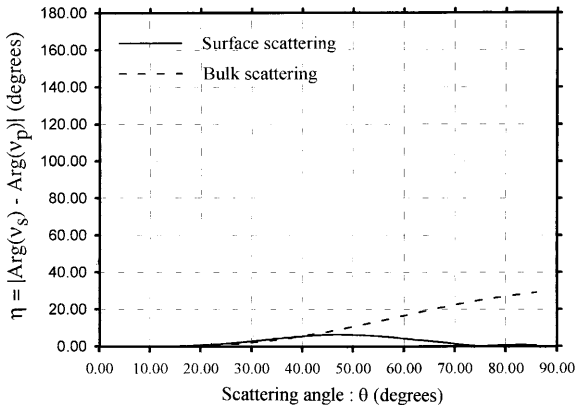


Fig. 8. Calculation of the scattering phase term $\eta(\theta)$ for a single Ta_2O_5 layer of optical thickness $8\lambda_0/4$, where $\lambda_0 = 633$ nm is the illumination wavelength. For surface calculation, the two interfaces are identical. The illumination incidence is $i = 0^\circ$. Surface and bulk scattering can be separated.

and the polarimetric phase difference of scattering is given by

$$\eta = \eta_s - \eta_p = \arg[C_0(s)] - \arg[C_0(p)]. \quad (43)$$

Relation (43) shows that the scattering phase term of a single surface does not depend on surface defects. The result is identical for scattering from a single bulk, in which h_0 is replaced by p_1 .

In the case of surface scattering from a multilayer, we know that, for most high-quality coatings produced on standard substrates (1-nm roughness), each interface roughness is identical to the substrate roughness h_p that is perfectly replicated within the stack.^{4,7,12,13} In this case, surface correlation is perfect and the same profile $h_i = h_p$ appears in Eq. (40). This result causes all structural terms to vanish again in the polarimetric phase given by

$$\eta = \eta_s - \eta_p = \arg\left[\sum C_i(s)\right] - \arg\left[\sum C_i(p)\right]$$

for perfect correlation. (44)

The result is identical for bulk scattering involving perfectly correlated inhomogeneities.

From these remarks we conclude that ellipsometric measurements do not allow us to characterize the geometry of the irregularities that are perfectly correlated, while they do allow us to detect the origin of these irregularities by means of the phase term η that depends on the C_i coefficients. In Fig. 8, for example, we compare the polarimetric phase term $\eta(\theta)$ calculated for surface scattering with the polarimetric phase terms $\eta(\theta)$ calculated for bulk scattering from a single layer. For surface scattering, the two interfaces are assumed to be perfectly correlated, whereas bulk scattering does not involve a correlation factor, as we have a unique bulk. Evidence is that the two effects (surface and bulk) can be separated by means of the ellipsometric phase term.

In Fig. 9 we give the calculation of the phase term

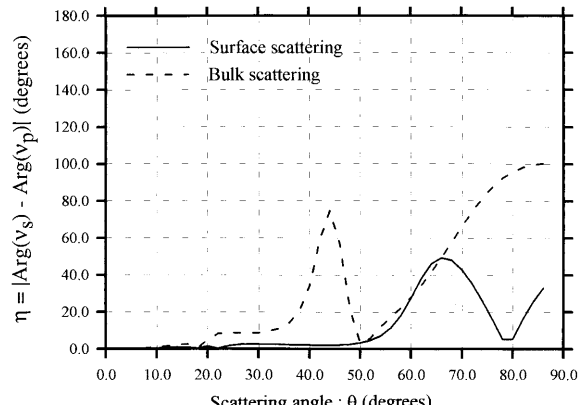


Fig. 9. Same as Fig. 8, except that the design is HLHLH(6L)HLHLH (see text), with materials TiO_2 and SiO_2 . All surface and bulk defects are perfectly correlated for this calculation.

$\eta(\theta)$ in the case of a coating with design HLHLH(6L)HLHLH, where H and L are high- and low-index quarter-wave layers at the illumination wavelength $\lambda_0 = 633$ nm. For this calculation all surface or bulk irregularities are perfectly correlated. As above, surface and bulk effects can be separated by means of the phase term $\eta(\theta)$.

The case of partial correlation is strongly different and causes the phase term to contain information relative to the geometry of structural defects. This point is discussed further in the text (Section 4).

E. Application to Experiment

The measurement technique is identical to that of Section 2, except that the illumination incidence angle (i) is fixed while the scattering angle θ varies.

In Fig. 10 we have plotted the angular measurements and calculation of the scattering phase $\eta(\theta)$ for a single layer of Ta_2O_5 produced by ion plating on a supersmooth (0.2-nm) glass substrate. The optical thickness of the layer is $8\lambda_0/4$, where $\lambda_0 = 633$ nm is the wavelength of measurements. First we observe

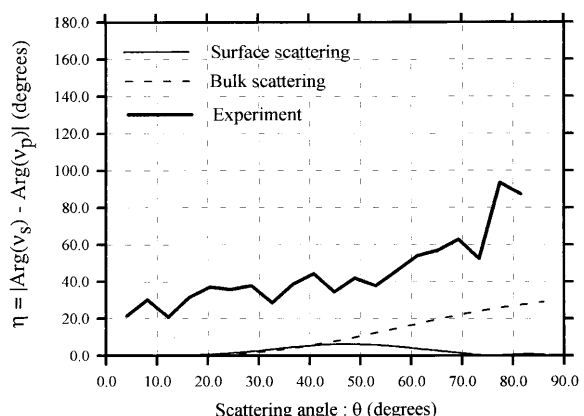


Fig. 10. Measurements at the 633-nm wavelength of the scattering phase term $\eta(\theta)$ for a single layer of Ta_2O_5 produced by ion plating. The calculation of Fig. 8 is also reported.

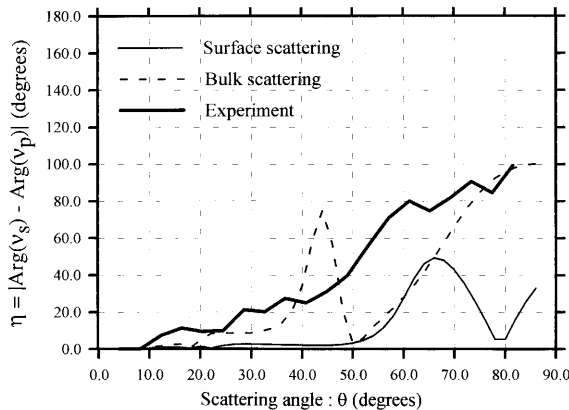


Fig. 11. Same as Fig. 10, but the sample is an 11-layer interference filter (see text). The calculation of Fig. 9 is also reported.

that the calculation of correlated surface or bulk scattering is rather far from the measurements. Moreover, the experimental data support strong variations in the angular range.

In the same way, we have measured the angular phase variations of an 11-layer interference filter produced by ion-assisted deposition, with materials TiO_2 and SiO_2 . This coating of design HLHLH(6L)HLHLH at 633 nm was deposited on a standard glass substrate (1-nm roughness). As shown in Fig. 11, the experimental data again do not really fit the calculation.

To understand these results, we first checked the quality of the experimental setup, and the repeatability of the measurements was found to be quasi-perfect in the angular range. We also checked the signal-to-noise ratio that can be critical for scattering ellipsometry on low-loss optics. Indeed a dynamic range $\Delta(F_{\max}, F_{\min})$ is necessary to measure the function $F(\phi)$, although F_{\max} decreases at increasing θ angles and therefore could cause F_{\min} to reach the detection level of the system. However, as shown in Fig. 12 for the multodielectric sample, the F function

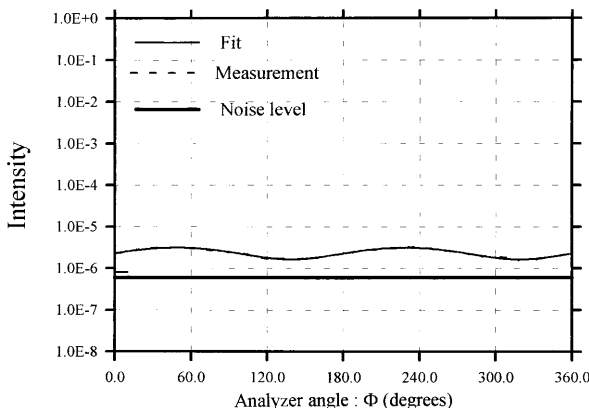


Fig. 12. Scattering measurements of $F(\phi)$ at $\theta = 72^\circ$ for the sample of Fig. 11. The experimental data are greater than the 7×10^{-7} system noise. The theoretical fit is superimposed on the measurements.

remains far from noise even at $\theta = 72^\circ$, which proves the quality of the measurements. The linearity of the setup was also shown to be perfect at these levels.

For all these reasons we cannot consider that the disagreement between measurement and calculation in Figs. 10 and 11 results from an artifact of the experimental setup. In fact, these anomalies result from a physical process, as discussed in Section 4.

4. Interpretation

A. Partial Correlation

In Figs. 8 and 9 the calculation is performed for correlated irregularities that describe identical defects at all surfaces and bulks. In this case the scattering phase is rather smooth and depends on only the origin of scattering, not on the geometry of irregularities (see Subsection 3.D). In fact, this case of perfect correlation is an extreme situation and any departure from it will modify the results of Subsection 3.D.

In the case of partial correlation,⁶ the polarimetric phase must be written for surface scattering as

$$\eta = \arg \left[\sum C_i(s) h_i \right] - \arg \left[\sum C_i(p) h_i \right] \quad \text{with } h_i \neq h_j \text{ for } i \neq j. \quad (45)$$

In this situation the structural terms h_i do not vanish in the phase difference η that therefore includes additional information. This phase term involves the Fourier transform of surface profiles that may present strong variations when the scattering angle or spatial frequency varies.

This result can be investigated as follows. In fact, the phase term η is the argument of the product of fields scattered at different polarizations:

$$\eta = \arg(A_s \bar{A}_p), \quad (46)$$

where

$$A_s = \sum_i A_{is}, \quad A_p = \sum_i A_{ip}. \quad (47)$$

From Eq. (20) we obtain

$$\eta = \arg \left(\sum_{i,j} D_{ij} \gamma_{ij} \right), \quad (48)$$

where

$$D_{ij} = C_i^r(s) \bar{C}_j^r(p), \quad (49)$$

$$\gamma_{ij} = h_i \bar{h}_j \quad (50)$$

is the cross-correlation spectrum of surfaces (i) and (j).

Now if we define a cross-correlation coefficient α_{ij} as⁶

$$\gamma_{ij} = \alpha_{ij} \gamma_{jj} = \alpha_{ij} |\alpha_{jp}|^2 \gamma_{pp} \quad (51)$$

we obtain

$$\eta = \arg(L) \quad (52)$$

where

$$L = \sum_{i,j} D_{ij} \alpha_{ij} |\alpha_{jp}|^2. \quad (53)$$

From relation (53) the information carried by scattering ellipsometry can be clearly emphasized. When the surfaces are identical, $\alpha_{ij} = 1$ and the phase term depends on only the D_{ij} factors that characterize the origin of scattering. On the other hand, any departure from perfect correlation will change the phase term that therefore varies with the geometry of the irregularities. When the surfaces are partially correlated, α_{ij} may be a complex function with amplitude and phase variations that increase with its random nature. Such a result can be enough to explain the angular variations of η observed in Figs. 10 and 11.

Moreover, at low angles ($\theta \approx 0^\circ$) we know that $C_i'(s) \approx C_i'(p)$, so that L can be turned into

$$L = \sum_j |\alpha_{jp}|^2. \quad (54)$$

For perfect correlation, $\alpha_{ij} = 1$ and L is real, which causes η to be zero. On the other hand, for partial correlation ($\alpha_{ij} \neq 1$), the L factor is no longer real and η is not equal to zero. This last result may be enough to explain why the ellipsometric phase in Fig. 10 is not zero at low scattering angles.

These predictions can be tested by comparison of Figs. 10 and 11, which correspond to coatings deposited on a supersmooth (0.1-nm roughness) and on a standard (1-nm roughness) glass substrate, respectively. In Fig. 10 correlation is most probably partial because of the supersmooth substrate, which explains angular variations in the phase together with a nonzero phase at low angles. On the other hand, correlation is close to unity in Fig. 11 because of the rather rough substrate, with a resulting smoother curve and a zero phase at low angles. These results appear to confirm the theoretical predictions.

B. Cross Polarization

Another reason for the disagreement between theory and experiment can be due to the presence of second-order terms in the scattering process that create cross-polarized light in the incidence plane. In this case first-order theory is responsible for disagreement because the phase term η cannot be zero at low θ angles, as shown below.

To take this effect into account, Eqs. (24) and (25) must be modified with $A_{sp} \neq 0$ and $A_{ps} \neq 0$. The result is an electric field after the analyzer, which is given by

$$\begin{aligned} A^* = & E_0^+ \cos(\psi - \alpha)[(\nu_{ss} \cos \psi + \nu_{ps} \sin \psi) \cos \phi \\ & + (\nu_{pp} \sin \psi + \nu_{sp} \cos \psi) \sin \phi], \end{aligned} \quad (55)$$

where ν_{ps} indicates *s*-polarized scattering that is due to *p*-polarized incident light.

Consequently, the resulting intensity can be calcu-

Table 1. Influence of Amplitude ρ of Cross-Polarization Ratio $\tau = \rho \exp(j\zeta)$ on the Determination of Scattering Phase Term η^a

$\rho = \rho'$	η (deg)
0	0
0.01	24.8
0.02	36.1
0.1	53.6
0.5	58.3

^aIn this case $\zeta = \zeta' = 0$.

Table 2. Influence of Argument ζ of Cross-Polarization Ratio $\tau = \rho \exp(j\zeta)$ on the Determination of Scattering Phase Term η^a

$\zeta = \zeta'$	η (deg)
10	44.4
20	35.4
50	8.7

^aIn this case $\rho = \rho' = 0.1$.

lated, with function F still given by relation (8) or (34), but parameters A , B , and C are given by

$$A = |\nu_{ss} \cos \psi + \nu_{ps} \sin \psi|^2, \quad (56a)$$

$$B = |\nu_{pp} \sin \psi + \nu_{sp} \cos \psi|^2, \quad (56b)$$

$$C = \text{Re}[(\nu_{ss} \cos \psi + \nu_{ps} \sin \psi)(\nu_{pp} \sin \psi + \nu_{sp} \cos \psi)]. \quad (56c)$$

In Tables 1 and 2 we illustrate the influence of amplitude cross-polarization ratio $\tau_{sp} = \nu_{sp}/\nu_{ss} = \tau_{ps}$ on the determination of polarimetric phase η . We observe that a scattering depolarization ampli-

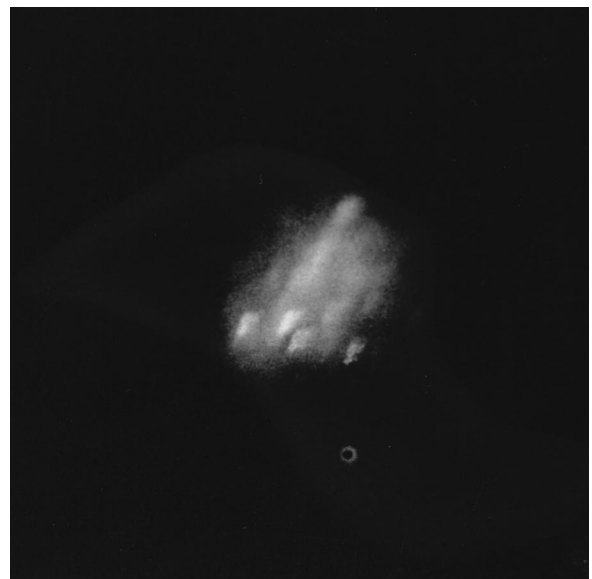


Fig. 13. Scattering photograph recorded at $\theta = 10^\circ$ on the sample of Fig. 11, with crossed polarizer and analyzer (image size 12 mm \times 8 mm).

tude ratio of 1% is enough to create a phase error of 25° on η . Moreover, this error also depends on the argument of τ . Obviously this error could be eliminated when the experimental data $F(\phi)$ are fitted with Eqs. (56) instead of Eqs. (35)–(37).

We conclude that such second-order cross-polarization terms can lead to nonzero values of the scattering polarimetric phase at low angles in Fig. 10. In Fig. 13 we present a photograph of the surface with a magnification $m \approx 10$ that confirms the existence of this effect, as it was realized at low θ angles with crossed polarizer and analyzer (s and p). In this situation, first-order theory predicts no cross-polarization, but the residual light passing through the analyzer originates from localized defects that can be seen in Fig. 13.

5. Conclusion

We have extended a previous scatterometer in order to build an angle-resolved ellipsometer with 10 axes that are fully computer controlled. The wavelength under study may vary from the UV to the mid-IR. With this experimental setup, reflection and scattering ellipsometric measurements can be performed. In the first step the apparatus was validated by means of classical specular ellipsometry measurements before it was used for diffuse ellipsometry at the 633-nm wavelength.

Scattering ellipsometric measurements were performed on single layers and multilayer coatings and revealed some effects that were not immediately under investigation. In particular the scattering ellipsometric phase may remain far from 0° at low scattering angles, and the experimental data support rapid variations in the θ angular range, which cannot be attributed to a lack of quality in the measurements.

When analyzing the equations for diffuse ellipsometry, we first observe that the polarimetric phase $\eta(\theta)$ is strongly connected with the origin of irregularities (surface or bulk). However, when these irregularities are perfectly correlated from one layer to another, this phase term carries information on only the origin of scattering, not on the geometry of the structural defects. In this case the phase term is smooth and zero at low angles. On the other hand, the case of partial correlation of the irregularities causes the polarimetric phase term to carry information relative to the geometry of the irregularities. In this situation the theoretical phase η is no longer smooth and no longer zero at low angles, which can be enough to explain all measurements. From these results one may find the ideal way of extracting precious information from ellipsometric measurements on light scattering.

Finally, we have shown that, because of the presence of second-order terms in the scattering process, cross-polarization factors appear in scattering ellipsometry equations. These terms are responsible for nonzero values of η at low angles. The cross-polarized light originates from localized defects in the coatings. Further information should be directly ob-

tained by the inclusion of such effects in scattering ellipsometry equations.

In a general way, ellipsometric measurements of light scattering appear to be a precious and complementary tool to analyze the scattering data. However, at this point, additional work on a simulation that involves partial correlation amplitudes and localized defects, together with experiments on rough and smooth substrates, should be done to definitely assess our conclusions.

References

1. J. M. Elson, J. P. Rahn, and J. M. Bennett, "Light scattering from multilayer optics: comparison of theory and experiment," *Appl. Opt.* **19**, 669–679 (1980).
2. J. M. Elson, J. P. Rahn, and J. M. Bennett, "Relationship of the total integrated scattering from multilayer-coated optics to angle of incidence, polarization, correlation-length, and roughness cross-correlation properties," *Appl. Opt.* **22**, 3207–3219 (1983).
3. J. M. Elson, "Theory of light scattering from a rough surface with an inhomogeneous dielectric permittivity," *Phys. Rev. B* **30**, 5460–5480 (1984).
4. C. Amra, "From light scattering to the microstructure of thin-film multilayers," *Appl. Opt.* **32**, 5481–5491 (1993).
5. A. Duparré and S. Kassam, "Relation between light scattering and microstructure of optical thin films," *Appl. Opt.* **32**, 5475–5480 (1992).
6. C. Amra, "Light scattering from multilayer optics. Part A: investigation tools," *J. Opt. Soc. Am. A* **11**, 197–210 (1994).
7. C. Amra, "Light scattering from multilayer optics. Part B: application to experiment," *J. Opt. Soc. Am. A* **11**, 211–226 (1994).
8. S. Kassam, A. Duparré, K. Helm, P. Bussemer, and J. Neubert, "Light scattering from the volume of optical thin films: theory and experiment," *Appl. Opt.* **31**, 1304–1313 (1992).
9. C. Amra, "First-order vector theory of bulk scattering in optical multilayers," *J. Opt. Soc. Am. A* **10**, 365–374 (1993).
10. C. Amra, C. Grèzes-Besset, and L. Bruel, "Comparison of surface and bulk scattering in optical coatings," *Appl. Opt.* **32**, 5492–5503 (1993).
11. C. Amra, D. Torricini, and P. Roche, "Multiwavelength (0.45–10.6-mm) angle-resolved scatterometer or how to extend the optical window," *Appl. Opt.* **32**, 5462–5474 (1993).
12. C. Amra, J. H. Apfel, and E. Pelletier, "The role of interface correlation in light scattering by a multilayer," *Appl. Opt.* **31**, 3134–3151 (1992).
13. C. Amra, C. Grèzes-Besset, S. Maure, and D. Torricini, "Light scattering from localized and random interface or bulk irregularities in multilayer optics: the inverse problem," in *Optical Interference Coatings*, F. Abeles, ed., Proc. SPIE **2253**, 1184–1200 (1994).
14. R. M. A. Azzam and N. M. Bashara, *Ellipsometry and Polarized Light* (North-Holland, Amsterdam, 1977), pp. 364–416.
15. J. Rivory, "Ellipsometric measurements," in *Thin Films for Optical Systems*, F. Flory, ed. (Dekker, New York, 1995), pp. 299–328.
16. F. Abélès, "Quelques remarques au sujet de l'utilisation de méthodes optiques pour l'étude des matériaux, de leurs surfaces et interfaces," *Acta Electron.* **24**, 133–138 (1981).
17. C. Amra, M. Ranier, C. Grèzes-Besset, R. Mollenhauer, and G. Albrand, "Loss anomalies in multilayer planar waveguides," in *Optical Interference Coatings*, F. Abeles, ed., Proc. SPIE **2253**, 1005–1020 (1994).